Catalysis Today 149 (2010) 2–10

Contents lists available at ScienceDirect

Catalysis Today

journal homepage: www.elsevier.com/locate/cattod

Influence of the promoter's nature (nickel or cobalt) on the active phases 'Ni(Co)MoS' modifications during deactivation in HDS of diesel fuel

Bertrand Guichard [a,*], Magalie Roy-Auberger [a], Elodie Devers [a], Christophe Pichon [b], Christelle Legens [b], Philippe Lecour [b]

[a] IFP-Lyon, Direction Catalyse et Séparation, Rond-point de l'échangeur de Solaize, BP ñ 3, 69360 Solaize, France
[b] IFP-Lyon, Direction Physique et Analyse, Rond-point de l'échangeur de Solaize, BP ñ 3, 69360 Solaize, France

ARTICLE INFO

Article history:
Available online 28 April 2009

Keywords:
HDS
Mixed phase
Deactivation
Diesel
$Ni(Co)MoS_2$
Segregation

ABSTRACT

The characterization of various spent $Ni(Co)MoP/Al_2O_3$ catalysts has been performed in order to elucidate the active phase modifications undergone on the catalysts at operating conditions. Six catalysts coming either from industrial or pilot reactors were studied. The deactivation level (for hydrogenation reaction) can be determined by XPS analysis quantifying the 'Ni(Co)MoS' mixed phase amount. The spent catalyst active phases characteristics, at different levels of deactivation, firstly evidenced that the coke particularly influences the CoMo active phase (X-ray photoelectron spectroscopy) lowering the 'CoMoS' mixed phase amount. On the spent NiMo catalysts, most of the nickel is segregated (XPS, Extended X-ray Absorption Fine Structure, Transmission Electronic Microscopy/Energy Dispersive Spectroscopy) even after low residence time in the unit (pilot plant origin). In both cases it leads to the progressive deactivation of the catalyst. The coke does not seem to influence the 'NiMoS' mixed phase amount excepted at its life-end.

1. Introduction

Because of strengthening in environmental legislation, production of ultra-low sulfur diesel fuel became an essential issue for refiners. Catalysts used for hydrotreating are generally composed of sulfided molybdenum promoted by nickel or cobalt and supported on alumina. As indicated by Kasztelan et al. [1] hexagonal MoS_2 particles are formed and it is generally admitted that the active sites for HDS are located on the edges of the slabs [2]. Many analytical methods were developed to precisely describe the active phase ('Ni(Co)MoS') of hydrotreating catalysts. Some significant breakthroughs occurred during the last decade using Extended X-ray Absorption Fine Structure [3] (EXAFS). Today, this analytical methodology provides a guide to describe the local environment of MoS_2 crystallites by quantifying the rate of edge decoration with nickel [4] or cobalt [5]. In addition, recent improvements in XPS characterization led to quantify the sulfidation rate [3] and the proportion of 'CoMoS' phase [6,7] as well as the 'NiMoS' phase [8]. Crystallites of MoS_2 have been observed by several microscopic tools during the last decade. Three-dimensional structure of particles was recently investigated by De Jong et al. by HRTEM on $NiMo/Al_2O_3$ [9] or zeolite [10].

By 2009, the sulfur specification in diesel fuel will be decreased as low as 10 ppm. This level can be reached by hardening the working conditions (increase of temperatures, for example) or by using more active catalysts. In both cases, crucial questions are raised about catalyst stability including the active phase steadiness. The deactivation of the hydrotreating catalysts has been the subject of numerous studies [11–17]. Two main causes are generally invoked in the literature:

(1) The first one is the accumulation of coke inside the pores of the catalyst carrier which prevents reactive molecules from accessing the active sites. Most of the authors have shown that coke becomes more aromatic with processing time-on-stream [18–21] and turns to a graphite-like structure.
(2) The second cause of deactivation may be the modification of the active phase itself resulting from particles sintering [12] or segregation of the promoter initially in decoration of MoS_2 slabs [22–28]. Eijsbouts et al. [25] identified some big Ni_3S_2 bulk formed while processing $NiMo/Al_2O_3$ catalysts but did not observe such apparition during $CoMo/Al_2O_3$ aging. The results linked to the stability of MoS_2 edges are very controversial. Experimental studies by Breysse et al. [27,28] based on Mössbauer spectroscopy of spent CoMoS catalysts have revealed a loss of the mixed phase in reductive conditions while EXAFS investigation on $CoMo/Al_2O_3$ catalysts preformed by Yokoyama et al. [17] are not relevant with the promoter

* Corresponding author. Tel.: +33 4 78 02 56 08; fax: +33 4 78 02 20 66.
E-mail address: bertrand.guichard@ifp.fr (B. Guichard).

0920-5861/$ – see front matter © 2009 Elsevier B.V. All rights reserved.
doi:10.1016/j.cattod.2009.03.016

segregation. This suggests that the mixed phase stability highly depends on the working conditions.

The formation of coke on metallic sites of the catalyst has also been previously conceived [29] indicating the possible influence of coke on the mixed phase activity. In the case of nickel decoration, coking of particle edges becomes possible due to the ability of nickel to be coked as shown by Tracz et al. [30].

In a recent paper [31], it was shown that the active phase suffers deep modifications in working state. Coupling the DFT approach and the active phase characterizations (XPS and TEM), it led to suspect that the coke could interfere with the local MoS_2 environment. Nevertheless the crucial issue of the balance between the relative role of coking in one hand and segregation in another hand is still under question.

The promoter segregation and the loss of the active phase in working conditions are particularly addressed in this paper by performing XPS, EXAFS and TEM–EDX characterizations on selected freshly sulfided and spent catalysts. The possible deactivation scheme occurring during the catalyst life and as a function of reaction conditions is discussed by focusing on nickel and cobalt stability on the particles edges of MoS_2 crystallites.

2. Experimental

2.1. Catalysts samples

2.1.1. Spent catalysts

Several spent Ni(Co)MoP/Al_2O_3 catalysts have been selected for this work from two different origins. The first series (Ni-PP-A, Ni-PP-B, Ni-PP-E and Co-PP-A and Co-PP-B) come from pilot plants (PP) and correspond to an intermediate state of deactivation. The second series (Ni-IP-C and Co-IP-C) originate from industrial plants (IP) at the end of their lifetime. The samples collected from industrial plants were not protected from air exposure during the downloading. As a consequence, they could have been partially oxidized before the analysis. To consider all the samples in the same way, the pilot plant spent catalysts were collected in the same way. Before characterization and activity measurements in toluene hydrogenation, spent catalysts were washed with a toluene reflux at 523 K and dried at 5 kPa and 423 K. One NiMoP catalyst was collected after a pilot plant run and directly characterized after a download under argon, i.e. without any air exposure (Ni-PP-D) and then after 2 weeks air exposure (Ni-PP-E). All spent catalysts come from the same generation of fresh Ni(Co)MoP catalysts. They are presented in Tables 1 and 2.

2.1.2. Fresh catalysts

The oxide precursors of Ni-0 and Co-0 commercial catalysts were prepared impregnating a solution containing $(NH_4)_6[Mo_7O_{24}]\cdot 4H_2O$, $(NO_3)_2Ni\cdot 6H_2O$ (or $(NO_3)_2Co\cdot 6H_2O$), H_3PO_4 and H_2O_2 on a γ-alumina characterized by a high specific area (200 m^2/g) in order to obtain catalysts with the properties indicated in Table 3. The catalysts precursors were then dried and subsequently calcined at 773 K under air.

Table 1
Origin of different aged NiMoP/Al_2O_3 catalysts.

Origin	Feedstocks	Processing time (days)	Catalyst name
Fresh	–	0	Ni-0
Pilot plant	SRGO	47	Ni-PP-A
	VGO	31	Ni-PP-B
	Anthracene and phenylcarbazole + DMDS	5	Ni-PP-D
			Ni-PP-E
Industrial plant	GO	730	Ni-IP-C

Table 2
Origin of different aged CoMoP/Al_2O_3 catalysts.

Origin	Feedstocks	Processing time (days)	Catalyst name
Fresh	–	0	Co-0
Pilot plant	SRGO	25	Co-PP-A
	HGO	15	Co-PP-B
Industrial plant	GO	730	Co-IP-C

2.1.3. Sulfided catalysts

The oxide precursors NiMo (Ni-0) and CoMo (Co-0) were sulfided under model molecules in a continuous fixed-bed co-current upflow reactor. The feed, composed of cyclohexane (74.12%, w/w), toluene (20%, w/w) and dimethyldisulfide (5.88%, w/w), was fed into the reactor at a LHSV of 4 h^{-1} and a pressure of 6 MPa. Hydrogen was supplied with a ratio $H_2/HC = 450Nl\ l^{-1}$. Temperature was raised from 273 to 623 K with a 2-K/min ramp. A 5-h step was observed before cooling the reactor to 423 K. At this stage, all fluids were stopped. The catalysts were downloaded from the reactor and transferred to XPS pre-chamber without any exposure to the air. The catalysts obtained are named Ni-Sulf-0 and Co-Sulf-0.

2.2. Analytical method

The spent catalysts, as referenced in Tables 1 and 2, washed in toluene reflux and dried, were analyzed without further treatment after air exposure. The pretreatment described in Section 2.1.1 did not lead to an extent metal oxidation. Besides, non-published works carried out in IFP showed that the coke formed inhibited the oxidation of MoS_2 particles. Fresh catalysts described in Table 3 were presulfided before characterization and then analyzed without air exposure.

XPS measurements have been performed with an Axis Ultra-Kratos spectrometer using monochromatic Al Kα radiation ($h\nu$ = 1486.6 eV) and equipped with a hemi-spherical analyzer operating at fixed pass energy of 40 eV. The spot size on the sample was 700 μm × 300 μm. The recorded photoelectron binding energies were referenced against the C 1s contamination line at 284.6 eV. The XPS spectra of Mo 3d, Ni 2p, S 2p, Al 2p, P 2p, O 1s were recorded and analyzed using casaXPS software Version 2.0.71 after applying a Shirley background substraction and Gaussian (30%)–Lorentzian (70%) decomposition parameters.

The presulfided samples were prepared in a glove box under argon atmosphere. The powder was deposited and fixed on a

Table 3
Composition of fresh catalysts oxides and spent catalysts (XRF).

Catalysts	NiO (wt%)	CoO (wt%)	MoO_3 (wt%)	P_2O_5 (wt%)
Ni-0	2.6	–	15.0	6
Ni-PP-A	2.4	–	14.0	nd
Ni-PP-B	2.4	–	13.2	nd
Ni-IP-C	1.9	–	12.1	nd
Ni-PP-D	2.4	–	13.5	nd
Ni-PP-E	2.4	–	13.5	nd
Co-0	–	4.0	18.0	4
Co-PP-A	–	3.6	15.9	nd
Co-PP-B	–	3.3	15.2	nd
Co-IP-C	–	3.3	14.9	nd

sample holder and transferred into the spectrometer without exposure to air.

The methodology for the decomposition of $CoMoP/Al_2O_3$ spectra set up by Gandubert et al. [32] was applied to the present study of spent $CoMoP/Al_2O_3$ catalysts. The same kind of methodology is achieved in this work to evaluate the composition of the $NiMoP/Al_2O_3$ catalysts active phase. Spectra decomposition examples are reported in Fig. 1. For more data, refer to a previous paper [31].

The XPS decomposition led to the quantification of the absolute amount of each species as follows:

$$[j] = \frac{A_j/S_j}{\sum_{i=1}^{i=n} A_i/S_i} \times 100 \quad (1)$$

where A_i is the measured area of the species i, S_i is the sensitivity factor of the atom related to the species i (furnished by the manufacturer) and $[j]$ is the absolute amount of the specie j.

From the absolute amounts of the various species, the promotion rate which is defined as the percentage of Ni(Co) atoms engaged into the mixed "Ni(Co)MoS" phase, relatively to the total amount of Ni(Co) in the freshly sulfided sample Eq. (2) can be calculated:

$$PR = \frac{[Ni(Co)MoS]}{[Ni(Co)]_0} \times 100 \quad (2)$$

where 0 refers to the freshly sulfided sample.

We distinguish the promotion rate from the promoter ratio. The promoter ratio is defined as the Ni(Co)/Mo ratio in the slabs Eq. (3):

$$\left(\frac{Ni(Co)}{Mo}\right)_{slabs} = \frac{[Ni(Co)MoS]}{[MoS_2]} \quad (3)$$

To perform TEM analysis, the powdered catalysts were dispersed in ethanol. Two droplets of the solution were deposited on a Cu grid and dried. The sample was covered by a thin layer of an epoxy resin to prevent charging during TEM analysis. Shortly after preparation, the sample was analyzed with a FEI Tecnai FEG microscope with a 200 kV electron beam and equipped with an EDAX Energy Dispersive Spectrometer. MoS_2 morphology was studied by TEM

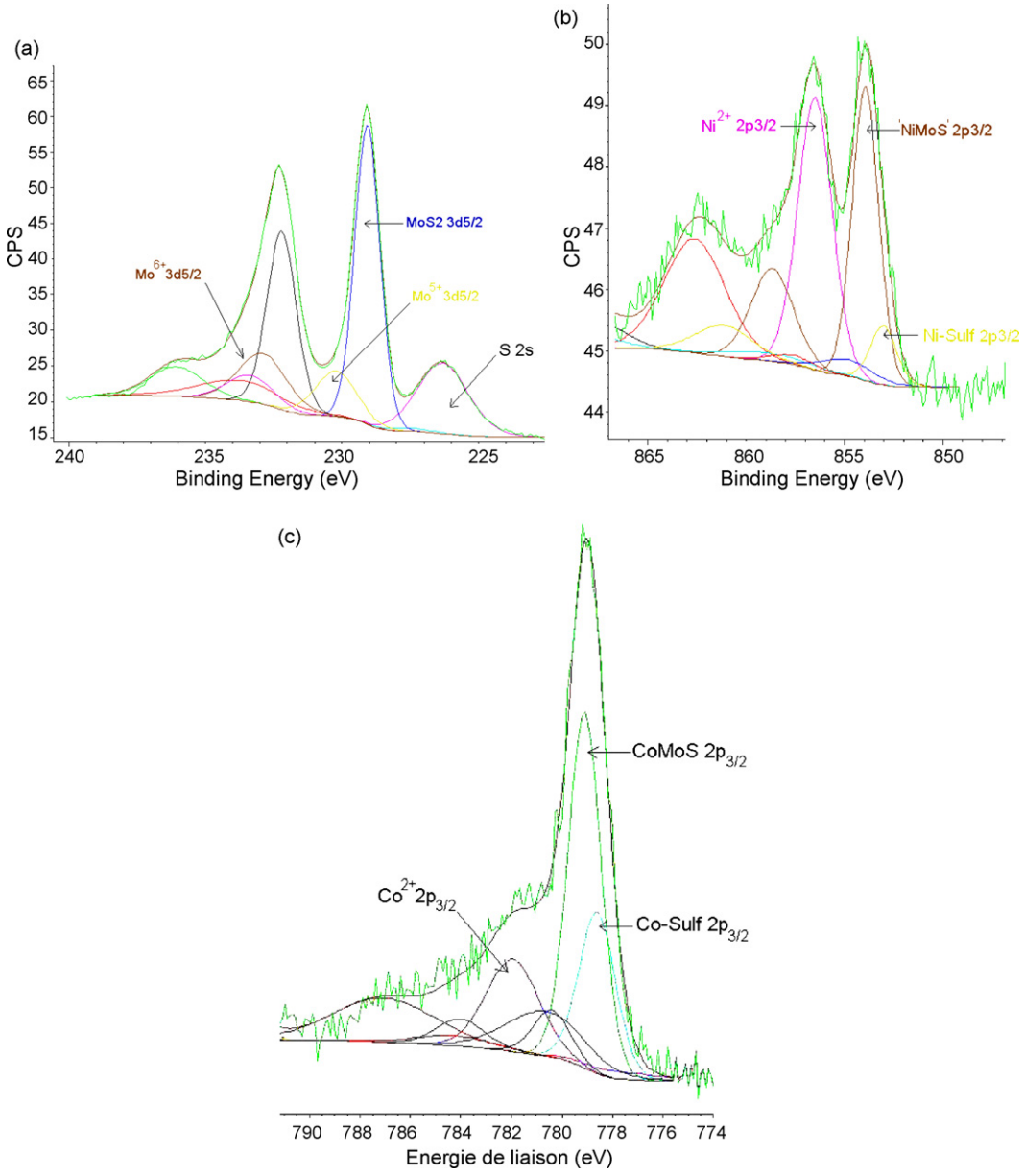

Fig. 1. XPS decomposition: (A) Mo 3d, (B) Ni 2p and (C) Co 2p.

imaging in the bright field mode. At least 15 micrographs (each corresponding to ca. 4000 nm^2) were evaluated for each sample. Semi-quantitative estimation of the MoS_2 feature was carried out by observing ca. 350 particles for each catalyst. The promoter segregation was investigated by TEM–EDX detection under analytical probe (1.0 nm) conditions, leading to Ni(Co)/Mo ratio calculated for about 20 particles. Ni–K, Co–K and Mo–K lines were used for this analysis. Such analysis could lead to partial reduction of the molybdenum sulfide [33]. This is why it is difficult to evaluate the error of the measurement, which is estimated to be ±20%rel.

XRF analysis were also performed and provided information on the overall composition of each catalyst.

EXAFS were performed at HASYLAB laboratory using DORIS III, a storage ring operated with an electron energy of 4.45 GeV and a current of 120 mA. Data were collected on the X1 station, a beam line placed after a bending magnet which is equipped with a double crystal monochromator, Si(1 1 1) for the Co or Ni–K-edges (7709 or 8333 eV, respectively) and Si(3 1 1) for the Mo–K-edge (20,000 eV). Measurements were done in transmission mode using ionisation chambers filled with krypton to absorb around 30% of the X-ray beam in the first ion chamber, around 40% of the X-ray beam in the second ion chamber and the remainder of the X-ray beam in the third ion chamber (used for online recording of reference spectra obtained from metallic foils of Co, Ni or Mo).

At Co–K-edge, the spectrum was recorded five times with a step of 2 eV (from 7559 to 8709 eV) and 2 s per point. At Ni–K-edge, the spectrum was recorded five times with a step of 2 eV (from 8183 to 9333 eV) and 2 s per point. At Mo–K-edge, each spectrum was recorded twice with a step of 3 eV (from 19,850 to 21,000 eV) and 2 s per point. The energy/angle calibration was performed using either a Co or Ni or Mo foil (various thicknesses) as references. Done the sieving, particles in the 100–200 μm range were pressed and loaded into a sample holder sealed by self-adhesive tape made of Capton®. The EXAFS spectra were recorded at room temperature under atmospheric pressure.

Fourier transforms (FT) of the k^3 weighted EXAFS functions were obtained using a Hanning type window ranging between 3.70 and 10.70 $Å^{-1}$ beyond the Co–K-edge, between 3.70 and 11.70 $Å^{-1}$ beyond the Ni–K-edge and between 3.10 and 13.1 $Å^{-1}$ beyond the Mo–K-edge (the spectra are noisy above those limits). In this whole work, all FT are calculated and presented without a phase correction. The inverse FT were obtained in the range between 0.90 and 3.60 Å for cobalt, between 0.90 and 3.50 Å for nickel and between 1.30 and 3.60 Å for molybdenum. EXAFS analysis was performed using the software package Athena-Artemis [34] and following the recommended procedures from the literature [35]. Cubic splines were used to obtain a smooth atomic background and to extract the EXAFS function. EXAFS data analysis was performed with theoretical backscattering phases and amplitudes calculated with code FEFF6 [36]. Structural parameters (interatomic distance) of the theoretical references used in this study are summarized in Table 4. A multi-shell least-squares fitting procedure (in *R*-space) using a single scattering EXAFS formulation was used to extract the co-ordination number (*N*), distance (*R*) and Debye–Waller factor ($\Delta\sigma$). Note that the numerical simulation corresponds to a typical residual in the order of 10–2.

2.3. Activity measurements

The hydrogenation activity of the spent catalysts was determined using toluene hydrogenation as a model reaction, in a continuous fixed-bed reactor. Experiments were carried out at 623 K and 6 MPa over 4 cm^3 of catalysts. The feed and reaction products were analyzed by FID gas chromatography with an apolar CP-SIL 5CB column. The first order activity was expressed relatively to the molybdenum amount.

Table 4
Structural parameters (interatomic distance) of the theoretical references used for EXAFS data analysis.

K-edge	Neighbors			
	S	Ni	Mo	Co
Mo	0.240 nm	0.285 nm	0.320 nm	0.294 nm
Ni	0.280 nm	0.300 nm	0.310 nm	–
Co	0.219 nm	–	0.316 nm	0.292 nm

3. Results and discussion

3.1. Catalysts activity measurements

Activity tests have been performed in a fixed-bed unit carrying out in situ sulfidation (during the catalyst heating). The toluene conversion leads to the hydrogenating performances of the various tested catalysts. The first order activities are respectively found to be 0.33 and 0.19 h^{-1} g_{Mo}^{-1} on fresh NiMoP and CoMoP catalysts. The spent catalysts performances, relative to the fresh catalyst one reported in Fig. 2 (NiMo catalysts) and Fig. 3 (CoMo catalysts) indicates a progressive deactivation with lifetime. At comparable lifetime, it is surprising that the CoMo catalysts exhibit lower relative activity loss than the NiMo ones. After pilot plant test the CoMo activity has been decreased by 10–40% against 50% for the NiMo while, after industrial runs, the CoMo catalyst still exhibits 40% of the initial activity whereas the NiMo one is only about 15%.

3.2. Size and stacking changes

The evolution of stacking and size of catalyst particles occurring during catalyst life has been characterized by means of TEM measurements (shown in Table 5). Even on a completely deactivated catalyst (Ni-IP-C), there is no effective modification

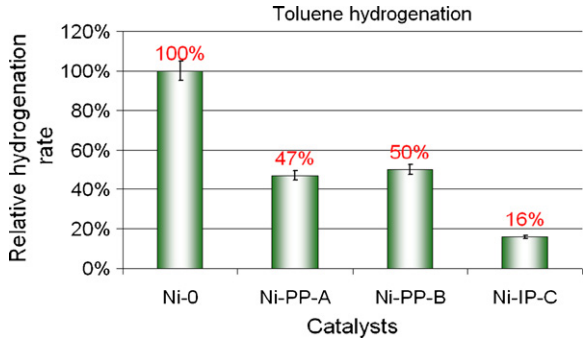

Fig. 2. Activities (first order kinetic approximation) (toluene hydrogenation) of spent NiMoP catalysts normalized with activity of fresh catalyst.

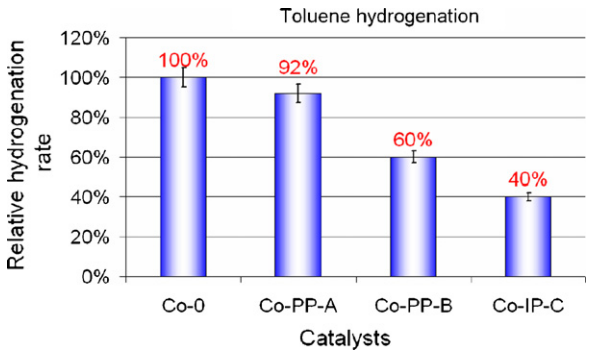

Fig. 3. Activities (first order kinetic approximation) (toluene hydrogenation) of spent CoMoP catalysts normalized with the activity of fresh catalyst.

Table 5
Stacking and average sizes measured by TEM analysis.

Origin	Catalyst name	Stacking	Size (nm)	Ni(Co)/Mo[a]		
				Average	Min	Max
Reference	Ni-Sulf-0	1.9 ± 0.9	3.7 ± 1.4	0.23	0.17	0.29
Spent	Ni-PP-A	1.8 ± 0.9	3.6 ± 1.6		nd	
	Ni-PP-B	1.8 ± 0.8	4.2 ± 1.9	0.12	0.05	0.18
	Ni-IP-C	1.5 ± 0.7	3.7 ± 1.6	0.12	0.03	0.22
Reference	Co-Sulf-0	2.5 ± 1.2	3.5 ± 1.7	0.20	0.12	0.29
Spent	Co-PP-A	1.6 ± 0.9	3.6 ± 1.5	0.20	0.09	0.48
	Co-IP-C	1.8 ± 1.5	4.1 ± 2.1	0.10	0.06	0.24

[a] Ratio in MoS_2 particles by EDX measurements.

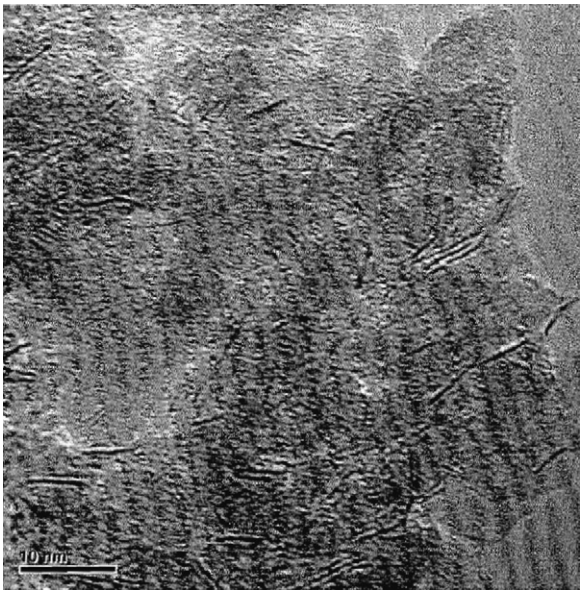

Fig. 4. TEM image on spent catalyst Ni-IP-C.

of the MoS_2 crystallites morphology, which suggests that the deactivation previously observed is not linked to MoS_2 sintering. It is also noted that the particles size (closed to 3.8 nm) and stacking (about two slabs) do not change with the promoter type (Ni or Co), which indicates that the stacking and size of MoS_2 sheets do not depend on the promoter nature.

An example of TEM images is presented in Fig. 4 for the Ni-IP-C case. Images are similar for all spent catalysts and we did not evidence the formation of Ni_3S_2-like or Co_9S_8-like crystallites of size greater than 1 nm (visible by TEM).

3.3. Chemical composition of the active phase

We have also coupled TEM observations with an EDX analyzer in order to evaluate the average chemical composition of the MoS_2 slabs. The average Ni–Mo or Co–Mo ratio obtained from the quantitative analysis of 20 MoS_2 slabs is reported in Table 5. The Ni–Mo ratio decreases from 0.23 on Ni-Sulf-0 to 0.12 on spent Ni-PP-B and Ni-IP-C, while no variation of the ratio is observed by X-ray fluorescence analysis. The tendency is not so clear when MoS_2 slabs are decorated with cobalt. Indeed the Co–Mo ratio appears steady (0.20) between Co-Sulf-0 and the one taken from pilot plant (Co-PP-B). The lower ratio seems to appear for higher processing times, reaching 0.10 on Co-IP-C. It might be proposed from EDX quantification and TEM observation that if the promoter segregates, it results to highly dispersed particles (beyond TEM resolution). Nevertheless the formation of such small aggregates cannot be totally excluded. Higher TEM resolution could have evidenced such formation.

For steady stacking and size features properties, it seems that the promoter amount in the MoS_2 crystallites decreases with processing time. We have intended to explore in more details this variation by performing XPS measurements.

The changes in Mo 3d, Ni 2p and Co 2p signals of spent catalysts have already been presented in a previous work [31]. It appeared that the promotion rate (calculated from Eq. (2)) and also the Ni(Co)/Mo ratio in the MoS_2 particles (calculated from Eq. (3)) decrease with processing time (Tables 6 and 7). The absolute amounts have been corrected with the bulk analysis (X-ray fluorescence) because the coke deposit can modify the composition by dilution of the XPS signal. To do so, the XRF values reported in Table 3 are used to estimate the expected nickel (or cobalt) amount:

$$[\mathrm{Ni(Co)}]_{\mathrm{expected}} = \frac{[\mathrm{Ni(Co)}]_{\mathrm{XRF}}}{[\mathrm{Ni(Co)}]_{\mathrm{XRF\text{-}0}}} \times [\mathrm{Ni(Co)}]_0 \quad (4)$$

The measured amounts (reported in Tables 6 and 7), are lower than expected. As a consequence the initial promoter amount needs the addition of four components: 'Ni(Co)MoS', 'Ni(Co)-Sulf', '$Ni(Co)^{2+}$' and 'Ni(Co) deficiency', this last value 'Ni(Co) deficiency' being calculated as the difference between the total promoter amount found by XPS and the expected amount.

The relative proportion of promoter between these four 'components' is shown in Fig. 5. We observe that the relative mixed phase amount 'Ni(Co)MoS' decreases. It is attributed on one hand to the lower total amount of promoter and on the other hand, to the nickel (cobalt) segregation. At life-end, the cobalt deficiency (about 40%) is found to be higher than the nickel deficiency (about 20%). Moreover, the sum of Ni-Sulf and Ni^{2+} amounts increases drastically at NiMo catalyst life-end (+20%) whereas the sum of Co-Sulf and Co^{2+} amounts is not significantly modified on CoMo

Table 6
Promotion rate (PR) and metals repartitions by XPS over spent and freshly sulfided $NiMoP/Al_2O_3$ catalysts.

Origin	Catalysts name	PR (Ni)[a]	Ni (%abs.)	Mo (%abs.)	$(Ni/Mo)_{slabs}$ [b]	Mo repartition (%rel.)			Ni repartition (%rel.)			S repartition (%rel.)			$(Ni/Mo)_{tot}$ [c]
						MoS_2	Mo^{5+}	Mo^{6+}	NiSulf	Ni^{2+}	NiMoS	S-Sulf	SO_x	Sulfates	
Reference	Ni-Sulf-0	57%	0.96	1.63	0.43	76	14	10	20	24	56	93	7	0	0.59
PP	Ni-PP-A	20%	0.66	1.84	0.17	56	17	27	17	56	27	62	9	29	0.36
	Ni-PP-B	25%	0.70	1.87	0.21	59	18	23	18	49	33	61	9	30	0.37
	Ni-PP-D	16%	0.88	1.70	0.12	76	13	11	63	20	17	89	11	0	0.52
	Ni-PP-E	15%	0.67	1.63	0.18	51	32	17	12	66	22	58	4	38	0.41
IP	Ni-IP-C	10%	0.54	1.35	0.14	48	20	32	7	76	17	56	11	33	0.40

[a] Promotion rate calculated according to Eq. (2) with Ni-Sulf-0 as a reference.
[b] Ni–Mo ratio in the MoS_2 slabs calculated from XPS results (Eq. (3)).
[c] Ni–Mo total atomic ratio calculated from XPS results (Eq. (1)).

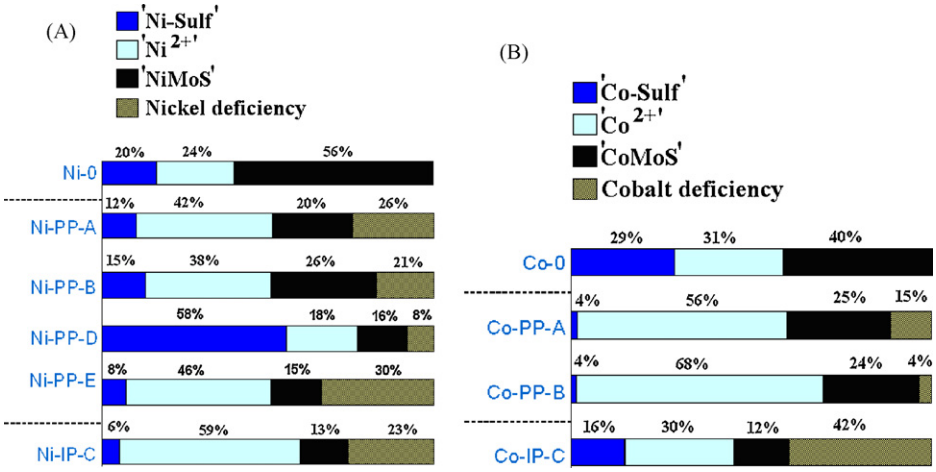

Fig. 5. XPS distribution of metals in freshly sulfided and spent NiMo catalysts (A) and CoMo catalysts (B).

Table 7
Promotion rate (PR) and metals repartitions by XPS over spent and freshly sulfided $CoMoP/Al_2O_3$ catalysts.

Origin	Catalyst name	PR (Co)[a]	Co (%abs.)	Mo (%abs.)	$(Co/Mo)_{slabs}$ [b]	Mo repartition (%rel.)			Co repartition (%rel.)			S repartition (%rel.)			$(Co/Mo)_{tot}$ [c]
						MoS_2	Mo^{5+}	Mo^{6+}	CoSulf	Co^{2+}	CoMoS	S-Sulf	SO_x	Sulfates	
Reference	Co-Sulf-0	40%	1.01	2.02	0.32	63	23	14	29	31	40	81	19	0	0.50
PP	Co-PP-A	23%	0.77	1.98	0.23	51	17	32	4	66	30	65	9	26	0.39
	Co-PP-B	20%	0.80	1.92	0.22	48	14	38	4	71	25	57	8	35	0.42
IP	Co-IP-C	10%	0.48	1.65	0.10	65	15	20	27	51	22	80	3	17	0.29

[a] Promotion rate calculated according to the Eq. (2) with Co-Sulf-0 as a reference sample.
[b] Co–Mo ratio in the MoS_2 slabs calculated from XPS results (Eq. (3)).
[c] Co–Mo total atomic ratio calculated from XPS results (Eq. (1)).

catalysts (+5 to 10%). It suggests that the NiMo and CoMo catalysts deactivate trough two different routes. It is quite evident that the nickel is highly segregated but at this stage of the work it is not possible to conclude on the cobalt segregation. Three hypotheses remain in order to elucidate the cobalt evolution:

- Cobalt aluminate formation.
- Coke deposit over the cobalt already segregated.
- Coke deposit over the cobalt in decoration (not segregated).

In order to quantify the influence of air exposure on the formation of oxidized species, we compared the XPS results obtained for Ni-PP-D and Ni-PP-E samples, respectively unloaded without any air exposure and after being exposed during 2 weeks air (Table 6 and Fig. 5). After air exposure (Ni-PP-E), the 'NiMoS' mixed phase proportion remains the same (15–16%) as before (Ni-PP-D). According to the variation of the other nickel chemical phases, it can be suggested that air exposure drives to the transformation of Ni-Sulf component into Ni^{2+} oxidized component and probably nickel sulfate species. Moreover, the nickel deficiency is artificially increased by air exposure, making the XPS interpretation harder, most probably due to the nickel sulfate increase. As a consequence, the 'Ni(Co)MoS' mixed phase amount observed by XPS is not influenced by the recuperation method (with air exposure). Nevertheless, the proportion of nickel hidden by coke is difficult to evaluate.

Concerning the amount of surface molybdenum on the spent catalysts determined by XPS (correcting as for nickel and cobalt using the XRF figures in Table 3), we do not observe the significant decrease as seen on the promoter signal. Three reasons may be invoked:

- The coke is deposited only over the MoS_2 edges and as a consequence selectively hides the promoter.
- The decrease of the promoter signal is due to coke deposits over the promoter already segregated.
- The promoter signal decrease is due to other reasons.

3.4. Nickel (cobalt) localization by EXAFS

In order to more precisely localize the promoter, and especially the cobalt, the catalysts were characterized by EXAFS. This technique should allow us to quantify the relative proportions of the effectively segregated nickel (cobalt) against the nickel (cobalt) hidden by the coke.

First of all, we focus on the NiMo catalysts in order to confirm the segregation occurrence. Fig. 6 presents the Fourier transforms of EXAFS Mo–K-edge spectra. Qualitative observations led us to note that the feature of Ni-PP-B and Ni-IP-C spectra are closed. The intensity of the first peak at 2.0 Å, corresponding to the sulfidation rate of molybdenum, is lower on the spent catalyst Ni-PP-C and Ni-IP-D spectra than on the fresh sample spectrum (Ni-Sulf-0). This could mean that the spent catalysts are slightly oxidized. Nevertheless the shape of the Fourier transform is kept similar to the

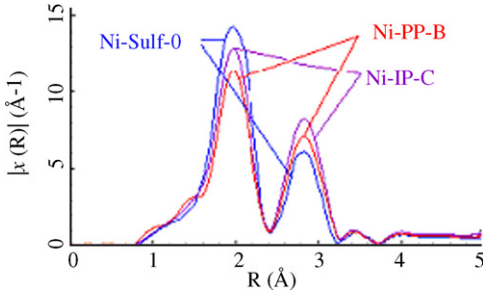

Fig. 6. Fourier transform of $NiMoP/Al_2O_3$ EXAFS spectra at the Mo–K-edge.

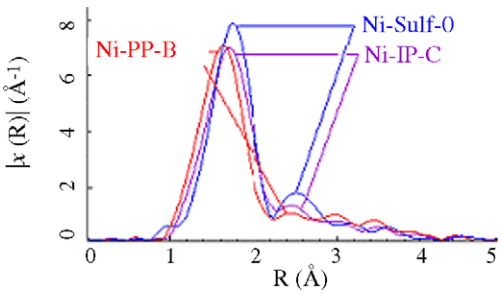

Fig. 7. Fourier transform of EXAFS spectra at the Ni–K-edge.

MoS_2 one and it can be said that the spent catalysts are only weakly oxidized. The second peak at 2.8 Å is attributed to Mo or Ni neighbors and should be modified due to the variations of both particles size and promotion rate. Indeed, the intensity seems to be higher on the spent catalysts, but it is not possible to conclude on the exact origin of the differences.

From the Ni–K-edge (Fig. 7) analysis, two main peaks are observed on the Fourier transforms. The first one, around 1.7 Å provides information on S, O and C neighbors. The downshift of this peak on both Ni-IP-C and Ni-PP-B compared to the fresh Ni-Sulf-0 is relevant to the nickel oxidation. In addition, the first peak distance decreases from Ni-IP-C to Ni-PP-B spectra, meaning that the nickel has been more oxidized on Ni-PP-B. The second peak at 2.4 Å is linked to nickel or molybdenum neighbors and will change according to the promotion ratio. This is why its intensity is very low on the spent catalyst and greater on the freshly sulfided catalyst, this last one being more promoted. Even if a slight oxidation can be observed on the spent catalysts, the Fourier transforms reveal a highly sulfided molybdenum.

After the qualitative observations, the spectra have been curve-fitted using the methodology described in Section 2, in order to go further in the results interpretation.

The Mo–K-edge fit parameters are firstly reported in Table 8. A high Mo–S coordination number was obtained on the freshly sulfided catalyst Ni-Sulf-0 (5.4), corresponding to a highly sulfided molybdenum. The Mo-S coordination number is lower on the spent catalyst Ni-PP-B (3.5) and Ni-IP-C (4.3). Both cases showed that the exposure to air destroys some part of the MoS_2 active phase, which is consistent with the previous results from XPS characterization. We confirm that Ni-PP-B is more oxidized than Ni-IP-C. Nevertheless, the Mo–S coordination number on the spent catalysts exposed to air shows that the molybdenum is still mainly sulfided. The Mo–Mo coordination number obtained is about 4.5 and is found to be similar on spent and fresh catalysts. Since the MoS_2 particles are hexagonal according to Kasztelan et al. [1] and more recently to Raybaud [37], it is possible to evaluate the particle size [38,39], which is found to be closed to 1.9 nm. As explained by Shido and Prins [38], this value underestimates the TEM measurement. Nevertheless it is confirmed that the particles size is not modified by aging. The Mo–Ni coordination number obtained on the freshly sulfided catalyst (Ni-Sulf-0) is about 1.2 while no Ni neighbor led to improve the fit of the spent catalyst spectra. As a consequence, it seems that the decoration rate is highly decreased during aging and that the promoter should have been segregated.

The segregation is confirmed by the curve-fits obtained with the Fourier transform at Ni–K-edge (Table 9). We found a Ni–Mo coordination number about 1.9 on the freshly sulfided catalyst, consistent with the "NiMoS" phase. Moreover we found a Ni–Ni coordination number about 0.9. This value evidences the formation of paired nickel atoms on the particles edges. On spent catalysts, no fit was relevant with experimental results. However, the main part of nickel is still largely sulfided (as previously indicated regarding the Fourier transform shape). Hence, it can be assumed that the nickel segregates from MoS_2 particles to form a nickel sulfide phase.

Table 8
EXAFS curve-fitting parameters at Mo–K-edge Fourier-filtered k^3-weighted EXAFS functions of the freshly sulfided and spent catalysts.

		N_{coord} (±0.5)	R (Å)	σ^2 ($\times 10^{-3}$ Å^2)	ΔE_0 (eV)
Ref.					
Ni-Sulf-0	S	5.4	2.41	4	−1.0
	Mo	4.5	3.19	12	−7.0
	Ni	1.2	3.11	2	5.1
Spent					
PP					
Ni-PP-B	S	3.5	2.40	3	0.7
	Mo	4.2	3.16	3	−1.3
	Ni	–	–	–	–
IP					
Ni-IP-C	S	4.3	2.40	4	0.3
	Mo	4.7	3.16	3	−1.5
	Ni	–	–	–	–
Ref.					
Co-Sulf-0	S	4.1	2.41	5	0.8
	Mo	1.7	3.15	5	−1.6
	Co	–	–	–	–
Spent					
PP					
Co-PP-B	S	1.8	2.41	3	5.7
	Mo	0.8	3.16	2	5.2
	Co	–	–	–	–
IP					
Co-IP-C	S	4.6	2.41	3	4.6
	Mo	3.0	3.16	4	−2.2
	Co	–	–	–	–

We now observe the CoMo catalyst Fourier transforms at Mo–K-edge (Fig. 8) and Co–K-edge (Fig. 9). The Mo–K-edge Fourier transform shape is similar to the one obtained with the NiMo catalysts. The high intensity of the first contribution shows that the fresh catalyst (Co-Sulf-0) is well sulfided. This intensity seems to

Table 9
EXAFS curve-fitting parameters at Ni–K-edge and Co–K-edge Fourier-filtered k^3-weighted EXAFS functions of the freshly sulfided and spent catalysts.

	N_{coord} (±0.5)	R (Å)	σ^2 ($\times 10^{-3}$ Å^2)	ΔE_0 (eV)
Ni-Sulf-0				
S	3.4	2.20	5	6.9
Mo	1.9	3.17	16	4.2
Ni	0.9	2.86	5	−8.7
Co-Sulf-0				
No curve-fitting				

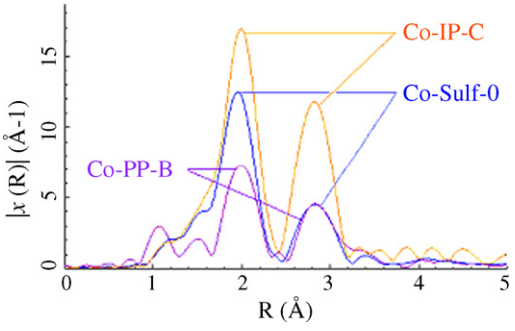

Fig. 8. Fourier transform of $CoMoP/Al_2O_3$ EXAFS spectra at the Mo–K-edge.

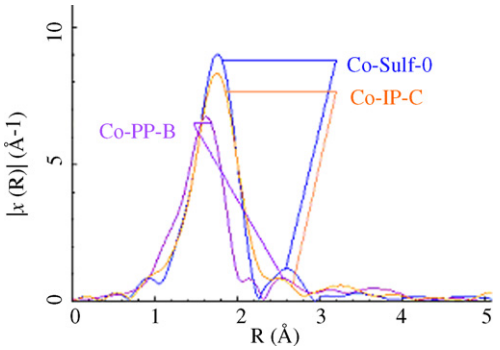

Fig. 9. Fourier transform of EXFAS spectra at the Co–K-edge.

be lower on the spent catalyst Co-PP-B. This sample is, thus probably highly oxidized. The low sulfidation rate of Co-PP-B is confirmed by the shape of the Co–K-edge Fourier transform (the first coordination sphere is highly downshifted compared to Co-Sulf-0). On the opposite, the Co-IP-C Fourier transform shapes at Mo–K-edge and Co–K-edge are not very different from the Co-Sulf-0 ones, which means that Co-IP-C seems to be still well sulfided.

The curve-fitting were performed on each Fourier transforms, following the methodology previously described in Section 2. The Mo–K-edge parameters are reported in Table 8. The Mo–S coordination number is about 4.1 on the freshly sulfided catalyst Co-Sulf-0. This value is slightly lower than the one found for the fresh Ni-Sulf-0 indicating that the sulfidation rate might be slightly lower than it is on Ni-Sulf-0. Surprisingly, the Mo–Mo coordination number is also very low on Co-Sulf-0. This sample might have been slightly oxidized inside the Kapton tape during the transfer from the glove bag where it is prepared to the analysis chamber. Nevertheless the Mo–S coordination number of Co-IP-C is about 4.6 and indicates that, even if it has been exposed to the air, this sample was not highly oxidized. Co-IP-C which seems to remain well sulfided exhibits a Mo–Mo coordination number closed to 3.0. It is different for Co-PP-B which exhibits only 1.8 as a Mo–S coordination number and 0.8 as Mo–Mo coordination number.

The analysis was completed by curve-fitting the Co–K-edge Fourier transforms. Even if the shapes of the spectra are clear due to some sulfided cobalt, it was not possible to elucidate the structure of the cobalt, which suggests that the three catalysts are poorly promoted. In the case of Co-Sulf-0 or Co-PP-B it could be due to oxidation, but in the case of Co-IP-C, well sulfided, it evidences that the mixed phase is not obtained. As a consequence, no significant difference is observed between the local environment of the freshly sulfided catalysts MoS_2 and the spent catalysts one. It can only be concluded that the cobalt segregation, if it occurs, is weak.

The thermodynamic stability study of both promoted edges [31,40] indicates that the HDS working conditions are not in favor of the nickel stability. This could explain why the amount of segregated nickel is so high at life-end. On the contrary, the cobalt seems to be more stable on S-edge, but it could also be more easily coked [31]. It is consistent with the final cobalt surface amount found by XPS and with the EXAFS values. The cobalt would not be segregated but might be hidden by the coke deposit over the particle edges.

At life-end, the "NiMoS" mixed phase amount is found to be very low and even lower than expected form DFT studies [40]. It could mean that the segregation is strengthened but the origin is not clear. We suspect the coke precursors to destabilize the nickel but we have no strong evidence.

Eventually, as reported in a previous work [31], the 'Ni(Co)MoS' amount is found to directly influence the hydrogenation activity of both systems (NiMo or CoMo) and the loss of the mixed phase could explain most of the catalyst deactivation.

4. Conclusion

This work compared the active phase characteristics of spent Ni(Co)MoP/Al_2O_3 catalysts at different levels of deactivation. We have intended to evidence the relative influence of coke deposit and promoter segregation in the deactivation scheme of both NiMo and CoMo HDS catalysts.

At this stage of the work and with the tools we have used, it is pointed out that the NiMo and CoMo catalysts deactivate trough two different routes. With cobalt, the deactivation originates mainly from the coke deposit although the segregation of the promoter and the modifications of the MoS_2 phase organization are more significant with nickel. The deactivation level (for hydrogenation reaction) can be determined by XPS analysis which allow to quantify the 'Ni(Co)MoS' mixed phase amount. At life-end, this amount is found to be very low and the coke could interfere in the deactivation scheme. As XPS analysis shows a slight promoter deficiency due to oxidation, it is not easy to precisely quantify the proportion of the promoter hidden by coke. The analysis directly performed after the download of the pilot plant catalysts should be considered to reach a better understanding of the deactivation mechanisms. Nevertheless this cannot be done also for industrial plant catalysts. Eventually, the better understanding of the catalyst deactivation drives to imagine some ways to prevent or at least reduce the catalyst aging.

Acknowledgements

The authors gratefully acknowledge L. Sorbier, A.L. Taleb, F. Moreau, and V. Lefebvre for TEM–EDX analysis and M. Corral-Valero for his contribution in the EXAFS characterization and fruitful discussions.

References

[1] S. Kasztelan, H. Toulhoat, J. Grimblot, J.P. Bonnelle, Appl. Catal. 13 (1984) 127.
[2] H. Topsøe, B.S. Clausen, F.E. Massoth, Hydrotreating Catalysis, Springer, Berlin, 1996, 29.
[3] T. Weber, J.C. Muijsers, J.H.M.C. Van Wolput, C.P.J. Verhagen, J.W. Niemantsverdriet, J. Phys. Chem. B 100 (1996) 14144.
[4] S.M. Bowens, D.C. Koningsberger, V.H.J. De Beer, S.A. Louwers, R. Prins, Catal. Lett. 5 (1990) 273.
[5] B.R.G. Leliveld, J.A.J. Van Dillen, J.W. Geus, D.C. Koningsberger, J. Phys. Chem. B 101 (1997) 11160.
[6] C. Legens, A. Gandubert, D. Guillaume, E. Payen, Surf. Interf. Anal. 38 (2006) 206.
[7] M. Karroua, H. Matralis, E. Sham, P. Grange, B. Delmon, Bull. Chem. Soc. Jpn. 68 (1995) 107.
[8] M. Nagai, T. Fukiage, S. Kurata, Catal. Today 106 (2005) 201.
[9] K.P. De Jong, L.C.A. Van Den Oetelaar, E.T.C. Vogt, S. Eijsbouts, A.J. Koster, H. Friedrich, P.E. De Jongh, J. Phys. Chem. B: Lett. 110 (2006) 10209.
[10] A.H. Janssen, A.J. Koster, K.P. De Jong, Angew. Chem. Int. Ed. 40 (2001) 1102.
[11] M. Marafi, A. Stanislaus, Symposium on catalysis in fuel processing and environmental protection, Presented Before the Division of Petroleum Chemistry, Inc. 214th National Meeting, American Chemical Society Las Vagas, NV, 1997.
[12] F. Pedraza, S. Fuentes, M. Vrinat, M. Lacroix, Catal. Lett. 62 (2007) 121.
[13] S.K. Song, S.K. Ihm, Korean J. Chem. Eng. 20 (2) (2003) 284.
[14] B.M. Vogelaar, A.D. Van Langeveld, S. Eijsbouts, J.A. Moulijn, Fuel 86 (7–8) (2007) 1122.
[15] B.M. Vogelaar, J. Gast, A.D. Van Langeveld, S. Eijsbouts, J.A. Moulijn, Petrol. Chem. Div. Preprints 47 (1) (2002) 77.
[16] B.M. Vogelaar, P. Steiner, A.D. Van Langeveld, S. Eijsbouts, J.A. Moulijn, Appl. Catal. A 251 (2003) 85.
[17] Y. Yokoyama, N. Shikawa, K. Nakanishi, K. Satoh, A. Nishijima, H. Shimada, N. Matsubayashi, M. Nomura, Catal. Today 29 (1996) 261.
[18] M.A. Callejas, M.T. Martinez, T. Blasco, E. Sastre, Appl. Catal. A 218 (2005) 181.
[19] S.K. Sahoo, S.S. Ray, I.D. Singh, Appl. Catal. A 278 (2004) 83.
[20] J.G. Weissman, S. Lu, B.M. Mc.Elrath, J.C. Edwards, Deactivation of hydrotreating catalysts, in: Proceedings of the 12th Canadian Symposium on Catalysis, Banff, Alberta, Canada, May 25–28, 1992.
[21] L.P.A.F. Elst, S. Eijsbouts, A.D. Van Langeveld, J.A. Moulijn, J. Catal. (2000) 95.
[22] M. Nagai, T. Arahata, Catal. Today 87 (2003) 123.
[23] S. Eijsbouts, Appl. Catal. A 158 (1997) 53.
[24] S. Eijsbouts, J.J.L. Heinerman, Appl. Catal. A 105 (1993) 69.
[25] S. Eijsbouts, L.C.A. Van Den Oetelaar, R.R. Van Puijenbroek, J. Catal. 229 (2005) 352.
[26] B.M. Vogelaar, P. Steiner, T.F. Van Der Zijden, A.D. Van Langeveld, S. Eijsbouts, J.A. Moulijn, Appl. Catal. A 318 (2007) 28.

[27] M. Breysse, R. Frety, B. Benaïchouba, P. Bussière, Radiochem. Radioanal. Lett. 59 (1983) 265.
[28] M. Breysse, R. Frety, M. Vrinat, P. Grange, M. Genet, Appl. Catal. 12 (2) (1984) 165.
[29] N. Martin, M. Viniegra, R. Zarate, G. Espinosat, N. Batina, Catal. Today 107–108 (2005) 719.
[30] E. Tracz, R. Scholz, T. Borowiecki, Appl. Catal. 66 (1990) 133.
[31] B. Guichard, M. Roy-Auberger, E. Devers, P. Raybaud, C. Legens, Catal. Today 130 (2008) 97.
[32] A. Gandubert, C. Legens, D. Guillaume, S. Rebours, E. Payen, Oil Gas Sci. Technol.-Rev. IFP 62 (1) (2007) 79.
[33] C. Glasson, C. Geantet, M. Lacroix, F. Labruyere, P. Dufresne, Catal. Today 45 (1998) 341.
[34] B. Ravel, M. Newville, J. Synchrotron Radiat. 12 (2005) 537.
[35] Y. Iwasawa, X-ray Absorption Fine Structure for Catalysts and Surfaces, London, world scientific 1996.
[36] J.J. Rehr, Rev. Mod. Phys. 72 (2000) 621.
[37] P. Raybaud, Appl. Catal. A 322 (2007) 76.
[38] T. Shido, R. Prins, J. Phys. Chem. B 102 (1998) 8426.
[39] C. Calais, N. Matsubayashi, C. Geantet, Y. Yoshimura, H. Shimada, A. Nishijima, M. Lacroix, M. Breysse, J. Catal. 174 (2) (1998) 130.
[40] E. Krebs, B. Silvi, P. Raybaud, Catal. Today 130 (2008) 160.